

Density-functional calculation of electronic friction of ions and atoms on metal surfaces

A. Liebsch

Institut für Festkörperforschung, Forschungszentrum Jülich, 52425 Jülich, Germany

(Received 16 July 1996)

The electronic friction of ions and atoms adsorbed on metal surfaces is calculated within the time-dependent density-functional approach. The metal is described within the jellium model and the nonlocal, short-wavelength response of the surface electrons is treated by using the adiabatic local-density approximation. The electronic friction is found to be considerably larger than in previous estimates that were based on not fully consistent descriptions of the creation of low-frequency electron-hole pairs. For Xe on Ag the friction parameter is $\eta_{\parallel} \approx 3.4 \times 10^8 \text{ s}^{-1}$, in good agreement with the values derived from quartz-crystal microbalance and surface resistivity measurements. These results confirm earlier suggestions concerning the important role of electronic processes in friction phenomena on metal surfaces. [S0163-1829(97)00919-3]

I. INTRODUCTION

Friction phenomena between macroscopic objects have been investigated for a long time.¹ Although this topic is of great technological importance, surprisingly little is known about the microscopic processes that give rise to the macroscopic friction force.² The recent availability of refined experimental techniques that can probe various contributions to the friction on an atomic scale^{3,4} has greatly stimulated the scientific interest in this phenomenon.

There are strong indications that during sliding the interaction of one or a few monolayers of lubrication molecules with the contact surfaces plays a crucial role. In the case of insulators, the microscopic friction necessarily involves the excitation of phonons while in metals excitation of both phonons and low-energy electron-hole pairs is feasible. The relative importance of electron and phonon channels on metals is still a controversial issue^{5,6} although very recent experimental and theoretical work suggests that on systems such as Xe on Ag, the electronic friction processes dominate.⁷⁻¹⁰

It is well known that the electronic excitations at metal surfaces depend very sensitively on the microscopic nature of the ground-state density distribution and on the nonlocal screening response to the time-varying external fields.¹¹ The aim of the present work is therefore to determine as accurately as possible the probability of creating electronic excitations via moving atoms and ions above a metal surface. The sliding friction of physisorbed atoms had been investigated previously using simple surface models.¹²⁻¹⁴ Persson and Volokitin⁹ improved these calculations by relating the friction coefficient to the surface response function $g(q, \omega)$ for which density-functional results are available.¹⁵ These early results of $g(q, \omega)$ were derived from an approximate expression of the effective surface potential that accounts for Coulomb but not exchange-correlation contributions. In view of the sensitivity of surface response properties to model assumptions, it seems therefore appropriate to perform improved response calculations that avoid this approximation.

In the present paper, the time-dependent local-density approximation¹⁶ (TDLDA) is used to evaluate the surface response function $g(q, \omega)$. In the adiabatic limit, this treat-

ment is equivalent to a self-consistent LDA description of the surface in the presence of a static external electric potential. The important result of these improved calculations is that the incorporation of exchange-correlation terms in the local potential makes the surface electronic density considerably more polarizable. Accordingly, the electronic friction parameters for physisorbed atoms are greatly enhanced. In the case of Xe sliding on Ag, we obtain $\eta_{\parallel} \sim 3.4 \times 10^8 \text{ s}^{-1}$. The calculated value is in qualitative agreement with the experimental results derived from surface resistivity measurements^{4,8} ($\eta_{\parallel} \sim 3 \times 10^8 \text{ s}^{-1}$) and from recent quartz-crystal microbalance data¹⁷ ($\eta_{\parallel} \sim 8 \times 10^8 \text{ s}^{-1}$).

The friction coefficients for the motion of ions near metal surfaces are also found to be much larger within the consistent description of the electronic surface excitations. In the case of K on Cu and Na on Al, we find $\eta_{\parallel} \sim 1.6 \times 10^9 \text{ s}^{-1}$ and $\sim 20 \times 10^9 \text{ s}^{-1}$, respectively. These results demonstrate the great sensitivity of surface excitation spectra to the electronic properties in the surface region and to the details of the nonlocal dynamical response to time-dependent external fields.

The outline of this paper is as follows. In Sec. II, the friction coefficients for atoms and ions, as well as the damping rate of adsorbed dipoles, are related to the surface response function $g(q, \omega)$. Section III summarizes the key aspects of the time-dependent density-functional approach. The low-frequency, short-wavelength excitations of metal surfaces are discussed in Sec. IV, which forms the main part of this work. In Secs. V and VI, these results are used to determine the electronic friction parameters of ions and atoms. A summary is given in Sec. VII, together with a suggestion for further theoretical work concerning realistic metal surfaces. Hartree atomic units are used throughout unless noted otherwise.

II. SLIDING FRICTION OF IONS AND ATOMS

Consider an ion or atom of mass M moving close to a metal surface. Because of the finite response time of the semi-infinite electron gas, the screening charge induced in the metal does not follow the particle motion adiabatically. As a result of this time lag the force acting on the particle at

a given time differs from its adiabatic value. The frictional force may be written as

$$\vec{f} = -M(\eta_{\parallel}\vec{v}_{\parallel} + \eta_{\perp}v_{\perp}\hat{z}), \quad (1)$$

where \vec{v} is the particle velocity and η_{\parallel} , η_{\perp} are the friction coefficients for the motion parallel and normal to the surface.

A. Ions

In the case of an ion of charge Q , the friction parameter η_{\perp} is given by the expression¹⁸

$$\eta_{\perp} = -\frac{Q^2}{M} \lim_{\omega \rightarrow 0} \frac{1}{\omega} \int d^3r \int d^3r' V(\vec{r}) \text{Im}\chi(\vec{r}, \vec{r}', \omega) V(\vec{r}'), \quad (2)$$

where $\chi(\vec{r}, \vec{r}', \omega)$ is the exact many-body density-density response function of the semi-infinite metal and $V(\vec{r})$ is defined as

$$V(\vec{r}) = \nabla_z \frac{1}{|\vec{r} - \vec{d}|}. \quad (3)$$

Here $\vec{d} = (0, 0, d)$ is the location of the particle relative to the surface. We assume the ion to be outside the electronic density of the metal. In this case, one has $\eta_{\perp} = 2\eta_{\parallel}$.¹⁹

In the following we describe the electronic properties of the metal in terms of the jellium model. Because of the translational invariance parallel to the surface it is convenient to use a two-dimensional Fourier representation. Expression (2) then simplifies to ($q \equiv |\vec{q}_{\parallel}|$)

$$\eta_{\perp} = \frac{Q^2}{M} \lim_{\omega \rightarrow 0} \frac{1}{\omega} \int_0^{\infty} dq q^2 e^{-2qd} \text{Im}g(q, \omega), \quad (4)$$

where

$$g(q, \omega) = -\frac{2\pi}{q} \int dz \int dz' e^{qz} \text{Im}\chi(z, z', q, \omega) e^{qz'} \quad (5)$$

is the so-called surface response function.^{20,21}

B. Atoms

In the case of a neutral physisorbed atom, the instantaneous mutual polarization of the atomic and metallic electron densities gives rise to the van der Waals attraction. If the atom is moving the finite response time of the metal leads to a friction force since the induced surface charge density lags behind.^{9,12,14} In principle, both the short-range repulsive and long-range attractive interactions can contribute to the friction force but we consider here only the damping caused by the van der Waals attraction. Thus we ignore all effects related to the overlap between the charge densities of metal and adsorbate.

As recently shown by Persson and Volokitin,⁹ the friction coefficient associated with the van der Waals attraction can be expressed as

$$\eta_i = -\frac{e^2}{M} \lim_{\omega \rightarrow 0} \frac{1}{\omega} \int d^3r \int d^3r' V_i(\vec{r}) \text{Im}\chi(\vec{r}, \vec{r}', \omega) V_i(\vec{r}'), \quad (6)$$

where the index $i = x, z$ refers to parallel or perpendicular motion of the atom, χ is again the density-density response function of the metal. The effective local interaction potential $V_i(\vec{r})$ is an approximate representation of the true non-local potential which results from the second-order processes involved in the transitions. Neglecting the electronic screening during the rapid intermediate virtual transitions, V_i may be written as

$$V_i(\vec{r}) \approx \alpha(0) \nabla_i \sum_j \left(\nabla_j \frac{1}{|\vec{r} - \vec{d}|} \right)^2 = \frac{\alpha(0)}{2} \nabla_i \frac{1}{|\vec{r} - \vec{d}|^4}. \quad (7)$$

Here $\alpha(0)$ is the static polarizability of the adatom and $\vec{d} = (0, 0, d)$ is the position relative to the surface.

Since $V_i(\vec{r})$ does not satisfy the Laplace equation, it can only be approximately represented in terms of a superposition of evanescent plane waves of the form

$$V_i(\vec{r}) = \sum_{q_{\parallel}} V_i(\vec{q}_{\parallel}) e^{iq_{\parallel} \cdot \vec{r}_{\parallel} + qz}. \quad (8)$$

The expansion coefficients are given by

$$V_i(\vec{q}_{\parallel}) = 2i\alpha(0) \int d^2q' q' \frac{\vec{q}' \cdot \vec{q}'' - q'q''}{q'q''(q+q'+q'')} Q'' e^{-(q'+q'')d}, \quad (9)$$

where $\vec{q}'' = \vec{q} - \vec{q}'$ and $Q'' = (\vec{q}'', -iq'')$. Inserting Eq. (9) into Eq. (6), one finds

$$\begin{aligned} \eta_i &= -\frac{e^2}{M} \lim_{\omega \rightarrow 0} \frac{1}{\omega} \sum_{q_{\parallel}} |V_i(\vec{q}_{\parallel})|^2 \\ &\quad \times \int dz \int dz' e^{qz} \text{Im}\chi(z, z', q, \omega) e^{qz'} \\ &= \frac{e^2}{M} \lim_{\omega \rightarrow 0} \frac{1}{\omega} \sum_{q_{\parallel}} |V_i(\vec{q}_{\parallel})|^2 \frac{q}{2\pi} \text{Im}g(q, \omega). \end{aligned} \quad (10)$$

Expressions (4) and (10) show that $\text{Im}g(q, \omega)$ is the central quantity that describes the microscopic electronic excitation processes that play a role in the sliding friction of atoms and ions near metal surfaces.

C. Vibrating dipoles

For completeness we note that the damping of adsorbate vibrations due to electronic excitations in the metal is closely related to the friction processes discussed above. For a dipole oscillating perpendicular to the surface at a frequency ω , the damping rate is given by²²

$$\tau^{-1} = -2 \int d^3r \int d^3r' V(\vec{r}) \text{Im}\chi(\vec{r}, \vec{r}', \omega) V(\vec{r}'), \quad (11)$$

with

$$V(\vec{r}) = \mu \nabla_z \frac{1}{|\vec{r} - \vec{d}|}, \quad (12)$$

and μ is the dynamic dipole moment. If the dipole is located outside the range of the equilibrium density of the metal, the damping rate can be expressed as

$$\tau^{-1} = 2\mu^2 \int_0^\infty dq q^2 e^{-2qd} \text{Im}g(q, \omega). \quad (13)$$

Thus, apart from the obvious prefactors, the vibrational lifetime is governed by the same surface loss function as the friction coefficients of atoms and ions.

III. TIME-DEPENDENT LOCAL DENSITY APPROACH

In order to evaluate the friction coefficients (4) and (10), an approximate expression must be found for the density-density response function $\chi(\vec{r}, \vec{r}', \omega)$. Since the ground state electronic properties of metal surfaces are rather accurately described within the local density approximation (LDA) of the exchange-correlation potential, the electronic excitations induced by the moving particle should be treated within a proper extension of the LDA. In the adiabatic version of the time-dependent local density approach,¹⁶ χ is expressed as a renormalized single-particle response function:

$$\chi(\vec{r}, \vec{r}', \omega) \approx \chi_1(\vec{r}, \vec{r}', \omega) + \int d^3 r_1 \int d^3 r_2 \chi_1(\vec{r}, \vec{r}_1, \omega) \times K(\vec{r}_1, \vec{r}_2) \chi(\vec{r}_2, \vec{r}', \omega), \quad (14)$$

where the interaction kernel consists of Coulomb and exchange-correlation contributions

$$K(\vec{r}, \vec{r}') = \frac{1}{|\vec{r} - \vec{r}'|} + V'_{\text{xc}}[n_0(\vec{r})] \delta(\vec{r} - \vec{r}') \quad (15)$$

and χ_1 represents the independent-electron response function

$$\chi_1(\vec{r}, \vec{r}', \omega) = \sum_{\vec{k}, \vec{k}'} (f_{\vec{k}} - f_{\vec{k}'}) \frac{\psi_{\vec{k}}^*(\vec{r}) \psi_{\vec{k}}(\vec{r}') \psi_{\vec{k}'}(\vec{r}) \psi_{\vec{k}'}^*(\vec{r}')}{\omega + \epsilon_{\vec{k}} - \epsilon_{\vec{k}'} + i\delta}. \quad (16)$$

Here $f_{\vec{k}}$ is the Fermi-Dirac distribution function and $\epsilon_{\vec{k}}$ and $\psi_{\vec{k}}(\vec{r})$ are the LDA single-particle energies and wave functions. These quantities include the microscopic aspects of the electronic properties of the semi-infinite metal. Schematically χ is given by (we momentarily drop all spatial arguments and integrals)

$$\chi = \chi_1 + \chi_1 K \chi_1 + \dots = \frac{\chi_1}{1 - K \chi_1}. \quad (17)$$

The virtue of the TDLDA approach is that the electron-electron interactions in the presence of the external perturbation are treated in the same manner as in the ground state, i.e., via the same local exchange-correlation potential $V_{\text{xc}}[n]$ derived from the homogeneous electron gas. In the adiabatic limit, this response treatment is equivalent to the self-consistent LDA ground state in the presence of a static electric field.

In principle, the exchange-correlation contribution to the interaction kernel K [the second term in Eq. (15)] should be of the more general form $f_{\text{xc}}(\vec{r}, \vec{r}', \omega)$,²³ i.e., it should be nonlocal and depend on frequency. The approximate form used in Eq. (15) is based on the following assumptions. (i) The true f_{xc} is replaced by the corresponding quantity of the homogeneous electron gas. In addition, both the ground state and induced densities are assumed to be slowly varying. These assumptions should be of a similar accuracy as the LDA in the ground state. The main problem of the local approximation is the failure to reproduce the asymptotic image potential. Since the image form, however, sets in at distances where the equilibrium density is rather small, nonlocal corrections are presumably not very important. (ii) The neglect of the frequency dependence excludes all correlation effects that go beyond a mere polarization of the electronic system. Processes such as double excitations or ionization are neglected. Since we are here concerned with near-adiabatic excitations, such finite-frequency corrections to K should be rather small. Under these assumptions it is justified to approximate

$$f_{\text{xc}}(\vec{r}, \vec{r}', \omega) \approx f_{\text{xc}}(q=0, \omega=0) \delta(\vec{r} - \vec{r}'), \quad (18)$$

where $f_{\text{xc}}(q=0, \omega=0) = V'_{\text{xc}}[n_0(\vec{r})]$ is derived from the homogeneous electron gas. This limit corresponds to the expression used in the second term of Eq. (15).

If the exchange-correlation contribution to the interaction kernel K is omitted, the response treatment corresponds to the random-phase approximation (RPA). This does not, however, amount to the time-dependent Hartree approximation as long as the ground-state properties are treated within the LDA. By RPA we therefore mean ‘‘LDA-based RPA.’’ This hybrid electron-electron interaction treatment violates certain sum rules that are satisfied in the TDLDA.²⁴ Obviously, this mixed LDA-RPA response treatment does not give the correct LDA ground state if the excitation frequency approaches the adiabatic limit. Since exchange-correlation terms tend to reduce the strength of the bare Coulomb interaction potential, the surface density profiles appear stiffer in the RPA than in the consistent TDLDA. As we will see below, for the low-frequency excitations that are relevant in friction phenomena, the RPA response treatment leads to significant underestimates of the probability of creating electron-hole pairs.

According to the approximation (14), the linearly induced surface charge density is given by

$$\begin{aligned} n_1(\vec{r}, \omega) &= \int d^3 r' \chi(\vec{r}, \vec{r}', \omega) \phi_{\text{ext}}(\vec{r}', \omega) \\ &= \int d^3 r' \chi_1(\vec{r}, \vec{r}', \omega) \phi_{\text{scf}}(\vec{r}', \omega). \end{aligned} \quad (19)$$

In this mean-field treatment, all many-electron correlations are incorporated in the effective or self-consistently screened complex local potential:

$$\phi_{\text{scf}}(\vec{r}, \omega) = \phi_{\text{ext}}(\vec{r}, \omega) + \phi_{\text{ind}}(\vec{r}, \omega), \quad (20)$$

where the induced potential is given by

$$\begin{aligned}\phi_{\text{ind}}(\vec{r}, \omega) &= \phi_{\text{est}}(\vec{r}, \omega) + \phi_{\text{xc}}(\vec{r}, \omega) \\ &= \int d^3r' K(\vec{r}, \vec{r}') n_1(\vec{r}', \omega).\end{aligned}\quad (21)$$

The electrostatic potential satisfies the Poisson equation

$$\nabla^2 \phi_{\text{est}}(\vec{r}, \omega) = -4\pi n_1(\vec{r}, \omega) \quad (22)$$

and the induced exchange-correlation potential is obtained from a Taylor expansion of the local ground-state exchange-correlation potential:

$$\phi_{\text{xc}}(\vec{r}, \omega) = V'_{\text{xc}}[n_0] n_1(\vec{r}, \omega). \quad (23)$$

Let us now consider the perturbation of the metal electrons caused by an external charge distribution. If these charges do not overlap with the metal electron density, the external potential is of the general form ($q \equiv |\vec{q}_{\parallel}|$)

$$\phi_{\text{ext}}(\vec{r}, t) = -\frac{2\pi}{q} e^{qz} e^{i(\vec{q}_{\parallel} \cdot \vec{r}_{\parallel} - \omega t)}. \quad (24)$$

The creation of electronic surface excitations via such a potential is determined by the golden rule formula

$$\begin{aligned}w(q, \omega) &= 2\pi \sum_{\vec{k}, \vec{k}'} f_{\vec{k}}(1 - f_{\vec{k}'}) |\langle \vec{k}' | \phi_{\text{scf}} | \vec{k} \rangle|^2 \\ &\quad \times \delta(\epsilon_{\vec{k}'} - \epsilon_{\vec{k}} - \omega).\end{aligned}\quad (25)$$

Because of screening processes, the amplitudes of the electronic transitions between the single-particle states are determined by $\phi_{\text{scf}}(\vec{r}, \omega)$ rather than the bare potential $\phi_{\text{ext}}(\vec{r}, \omega)$. The transition rate $w(q, \omega)$ may also be written in terms of the imaginary part of the surface response function defined in Eq. (5):²¹

$$w(q, \omega) = \frac{4\pi}{q} \text{Im}g(q, \omega). \quad (26)$$

Finally, using Eq. (19) it is evident that $g(q, \omega)$ may be obtained from the exponential moment of the induced density

$$g(q, \omega) = \int dz e^{qz} n_1(z, q, \omega). \quad (27)$$

Thus, there are two equivalent expressions that can be used to evaluate the surface excitation spectra: (i) the golden rule formula for the transition rate $w(q, \omega)$ that requires the complex local potential $\phi_{\text{scf}}(\vec{r}, \omega)$, and (ii) the surface loss function $\text{Im}g(q, \omega)$, derived from the spatial distribution of the induced surface charge density $n_1(\vec{r}, \omega)$. This density is related to the local potential ϕ_{scf} via the response equation (19).

It is clear from the above derivation that, in order to be consistent, the full ϕ_{scf} given by Eqs. (20) and (21) must be used in the evaluation of the golden rule formula. This consistency requirement had been overlooked in earlier calculations of the transition rate,^{15,21} where ϕ_{scf} in Eq. (25) was approximated as $\phi_{\text{ext}} + \phi_{\text{est}}$, even though the induced density was evaluated correctly within the LDA. This approxi-

mation differs from the RPA response which neglects the induced exchange-correlation potential ϕ_{xc} even in the calculation of n_1 .

IV. LOW-FREQUENCY, SHORT-WAVELENGTH EXCITATIONS

A. Transition rate

Taking advantage of the translational symmetry of jellium systems, the golden rule expression (25) can be simplified to²¹

$$w(q, \omega) = \frac{4}{\pi^3} \int d^3k f_{\vec{k}}(1 - f_{\vec{k}'}) \frac{1}{k_z} |\langle k'_z | \phi_{\text{scf}} | k_z \rangle|^2, \quad (28)$$

where $\vec{k}' = (k_x + q, k_y, [k_z^2 + 2\omega - 2k_x q - q^2]^{1/2})$. These relations follow from the conservation of the parallel momentum and of the single-particle energy during the electronic transition, i.e., $\epsilon_{\vec{k}'} = \epsilon_{\vec{k}} + \omega$. We take \vec{q}_{\parallel} along the x direction.

As a result of the occupation factors, the three-dimensional integral over \vec{k} may be further reduced as follows. First, we make use of the relation $\kappa_0^2 \leq k_y^2 \leq \kappa_1^2$, where $\kappa_0 = (k_F^2 - k_z^2 - k_x^2 - 2\omega)^{1/2}$ and $\kappa_1 = (k_F^2 - k_z^2 - k_x^2)^{1/2}$. k_F is the Fermi wave vector. Defining $\kappa = (k_F^2 - k_z^2)^{1/2}$, we have

$$\begin{aligned}I &\equiv \int d^3k f_{\vec{k}}(1 - f_{\vec{k}'}) \dots = \int_0^{k_F} dk_z \int_{-\kappa}^{\kappa} dk_x \int_{\kappa_0}^{\kappa_1} dk_y \dots \\ &\approx \int_0^{k_F} dk_z \int_{-\kappa}^{\kappa} dk_x \frac{2\omega}{\kappa_1} \dots\end{aligned}\quad (29)$$

The last identity follows from the expansion of $\kappa_1 - \kappa_0$ for small ω . Let us now introduce the variable φ via $k_x \equiv \kappa \cos\varphi$. Thus, $dk_x = -\kappa_1 d\varphi$ and

$$I = \int_0^{k_F} dk_z \int_0^{\pi} d\varphi 2\omega \dots \quad (30)$$

The transition rate (28) then takes the form

$$w(q, \omega) = \frac{8\pi}{k_F} \frac{\omega}{\omega_p} \xi(q), \quad (31)$$

where ω_p is the bulk plasma frequency and the coefficient $\xi(q)$ is defined as

$$\xi(q) = \frac{k_F \omega_p}{\pi^4} \int_0^{k_F} dk_z \int_0^{\pi} d\varphi \frac{1}{k'_z} |\langle k'_z | \phi_{\text{scf}} | k_z \rangle|^2. \quad (32)$$

This derivation shows that the linearity $w(q, \omega) \sim \omega$ arises purely from phase space factors. The remaining terms may therefore be evaluated in the static limit. Thus, $k'_z = (k_z^2 - 2\kappa q \cos\varphi - q^2)^{1/2}$ and $\phi_{\text{scf}} \equiv \phi_{\text{scf}}(z, q, \omega = 0)$. According to Eq. (26) the low-frequency behavior of the surface loss function is given by

$$\text{Im}g(q, \omega) = 2 \frac{q}{k_F} \frac{\omega}{\omega_p} \xi(q). \quad (33)$$

The quasistatic relation (31) is important since it shows that the near-adiabatic region of the surface excitation spectrum can be obtained from purely static response quantities.

We note however that the above derivation holds if the local potential ϕ_{scf} involves only short-range surface contributions. This does not apply in the small- q limit, where ϕ_{scf} acquires also long-range bulklike behavior because of the slow decay of e^{qz} . Such contributions give rise to additional terms in $w(q, \omega)$ that are also linear in ω (Ref. 21) (see below). Denoting the short-range surface part of ϕ_{scf} by ϕ_s , the corresponding linear coefficient of the transition rate in the small- q limit is given by

$$\xi_s = \frac{k_F \omega_p}{\pi^3} \int_0^{k_F} dk_z \frac{1}{k_z} |\langle k_z | \phi_s | k_z \rangle|^2, \quad (34)$$

with $\phi_s = \phi_{\text{scf}}(z, q=0, \omega=0)$.

B. Solution of response equation

Before evaluating the friction coefficients for ions and atoms we discuss in the remainder of this section the behavior of the transition rate $w(q, \omega)$ and of the linear coefficient $\xi(q)$. In practice we solve the response equation (19) for semi-infinite jellium surfaces by inverting the equation

$$n_1(z, q, \omega) - \int dz' \int dz'' \chi_1(z, z', q, \omega) K(z', z'', q) \times n_1(z'', q, \omega) = \bar{n}_1(z, q, \omega), \quad (35)$$

where the unscreened density induced by the bare external potential is given by

$$\bar{n}_1(z, q, \omega) = -\frac{2\pi}{q} \int dz' \chi_1(z, z', q, \omega) e^{qz'}. \quad (36)$$

The Fourier components of the response kernel are defined as

$$K(z, z', q) = -\frac{2\pi}{q} e^{-q|z-z'|} + V'_{\text{xc}}[n_0(z)] \delta(z-z'). \quad (37)$$

Discretizing all quantities on a mesh of points z_i , the response equation may be written in matrix form as

$$n_1 = (1 - \chi_1 W K w)^{-1} \bar{n}_1. \quad (38)$$

Here 1 denotes the unit matrix, $n_{1,i} = n_1(z_i, q, \omega)$, $\chi_{1,ij} = \chi_1(z_i, z_j, q, \omega)$, etc. The weight factors W_{ij} and w_{ij} must be chosen such that the cusps of χ_1 and K for $z = z'$ are dealt with accurately.

The Fourier components of the response function χ_1 are given by

$$\chi_1(z, z', q, \omega) = \frac{2}{\pi^3} \int_0^{k_F} dk_z \int_{-(k_F^2 - k_z^2)^{1/2}}^{(k_F^2 - k_z^2)^{1/2}} dk_x (k_F^2 - k_z^2 - k_x^2)^{1/2} \times \psi_{k_z}(z) \psi_{k_z}(z') [G(z, z', \epsilon_+) + G(z, z', \epsilon_-)], \quad (39)$$

where $\epsilon_{\pm} = \epsilon_{k_z} \pm (\omega + i\delta - k_x q) - q^2/2$. The functions $\psi_{k_z}(z)$ are the bound states of the semi-infinite metal and $G(z, z', \epsilon_{\pm})$ the corresponding Green's functions. Detailed definitions can be found in Ref. 25.

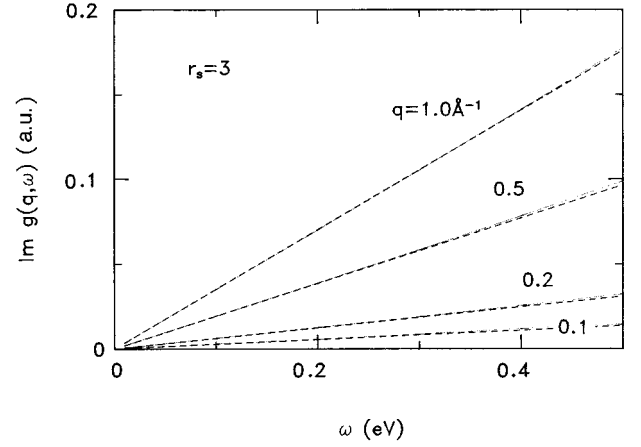


FIG. 1. Surface loss function $\text{Im} g(q, \omega)$ for semi-infinite jellium ($r_s = 3$) as a function of frequency for several parallel wave vectors. Solid curves, TDLDA results derived from Eq. (27); straight lines, quasistatic results derived from Eq. (33).

A crucial step is the evaluation of the unscreened induced density $\bar{n}_1(z, q, \omega)$ in Eq. (36). In the surface region, Simpson integration over z' is adequate. However, it is very important not to neglect the asymptotic range $z' \rightarrow -\infty$. This contribution can be taken into account using the asymptotic forms of the bound states and Green's functions. By performing first the z' and then the k_z, k_x integrations in χ_1 , one can do the z' integration analytically in the asymptotic region. In order to include the asymptotic region in the internal integration of $\chi_1 K$, the Coulomb kernel is written as

$$e^{-q|z-z'|} = e^{q(z-z')} + (e^{-q|z-z'|} - e^{q(z-z')}).$$

The integral over χ_1 times the first term on the right-hand side is related to the unscreened induced density \bar{n}_1 , i.e., the asymptotic region can be treated analytically as explained above. The integral over χ_1 times the term in parentheses is limited to $z > z'$ since this term vanishes for $z < z'$. The accurate handling of the asymptotic region ensures stability down to the adiabatic limit, a feature that is particularly important for low-frequency excitation phenomena.

C. Low-frequency excitations

Figure 1 shows the low-frequency behavior of the surface loss function $\text{Im} g(q, \omega)$ for several parallel wave vectors. These results are derived from TDLDA calculations of the induced density $n_1(z, q, \omega)$ and using the relation (27). The surface excitation spectra are seen to be linear in ω up to at least 0.5 eV independently of the value of q . The comparison with the corresponding results obtained from expression (33), with $\phi_{\text{scf}}(z, q, \omega)$ in Eq. (32) replaced by $\phi_{\text{scf}}(z, q, 0)$, demonstrates the remarkable accuracy of the quasistatic approximation.

The induced density $n_1(z, q, \omega)$ is shown in Fig. 2 for $q = 0.5 \text{ \AA}^{-1}$, $\omega = 0.5 \text{ eV}$. For smaller frequencies, the real part of n_1 is nearly independent of ω while the imaginary part decreases linearly. Thus, according to Eq. (27), the deviations of $n_1(z, q, \omega)$ from the static limit $n_1(z, q, 0)$ lead to

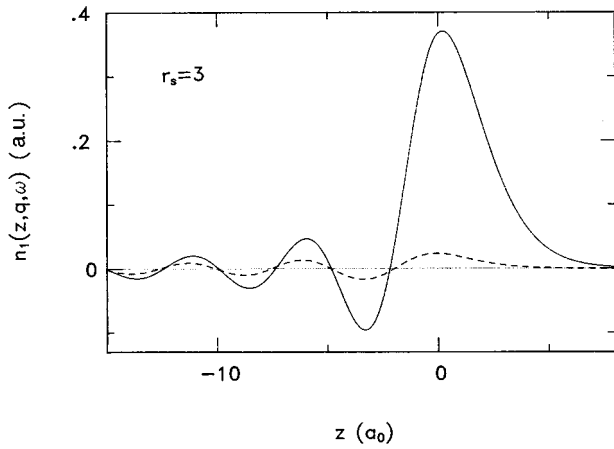


FIG. 2. Induced surface density $n_1(z, q, \omega)$ at 0.5 eV and $q = 0.5 \text{ \AA}^{-1}$, as calculated within the TDLDA ($r_s = 3$). Solid curve, real part; dashed curve, imaginary part.

contributions to $\text{Im}g(q, \omega)$ of $O(\omega^3)$. This behavior forms the basis for the validity of the quasistatic approximation.

In principle, the density induced at finite q and finite ω might exhibit also a propagating “bulk” contribution that vanishes in the adiabatic limit. Figure 3 shows the ω vs q region where bulk excitations are allowed. At small q , this continuum is limited by the line $\eta = \omega/(qv_F) = 1$, where v_F is the Fermi velocity. At the surface, the translational invariance is broken so that, at a finite \vec{q}_{\parallel} , bulk transitions may be generated even at frequencies where $\eta > 1$.

At small q and low ω such that $\eta = \omega/(qv_F) < 1$, the bulklike contribution to the transition rate increases like ω^5 .²¹ At the rather large q and small ω values of interest here, we have not been able to identify any propagating contribution to n_1 , even at large distances ($\sim 50 \text{ \AA}$) from the surface. Instead, the induced densities decay like $1/z^2$ towards the interior as expected from Friedel oscillations. In the evaluation of the surface response function $g(q, \omega)$, any bulklike components of the induced density would also be weighted by the factor e^{qz} , i.e., their long-range oscillatory behavior would be of no special consequence for the surface excitation spectra.

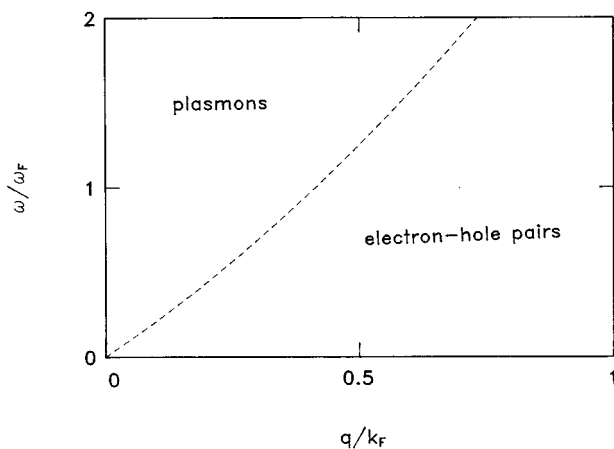


FIG. 3. Electron-hole continuum of three-dimensional electron gas. The boundary is determined by the function $q/k_F = (\omega/\omega_F + 1)^{1/2} - 1$, which approaches $\eta = \omega/(qv_F)$ for $q \ll k_F$.

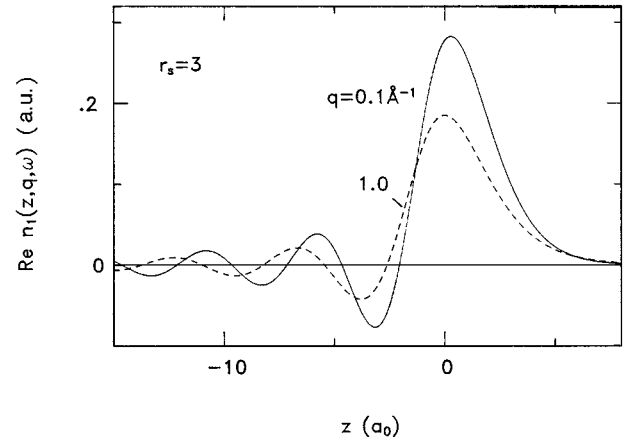


FIG. 4. Real part of normalized induced surface density $\bar{n}_1(z, q, \omega) = n_1(z, q, \omega)e^{-qz_1}$ at 0.1 eV as calculated within the TDLDA ($r_s = 3$). z_1 is the static image plane position. Solid curve, $q = 0.1 \text{ \AA}^{-1}$; dashed curve, $q = 1.0 \text{ \AA}^{-1}$.

Figure 4 shows the variation of the real part of the induced density with parallel momentum. Plotted are the normalized distributions $\bar{n}_1(z, q, \omega) = n_1(z, q, \omega)e^{-qz_1}$, where z_1 is the static image plane position in the limit $q = 0$. This normalization is chosen in order to compensate for the exponential increase of the external potential (24) near the centroid of n_1 . Because of the rather low frequency, these distributions are nearly identical to the corresponding static induced densities obtained previously using a coupled channels method.¹⁵ In the limit of small q , n_1 converges to the induced density calculated by Lang and Kohn²⁶ for uniform fields. At $q = 1.0 \text{ \AA}^{-1}$ the main peak has shifted towards the surface since higher density regions are involved in the screening of the applied field. Also, the wave vector of the Friedel oscillation increases according to $\alpha = (4k_F^2 - q^2)^{1/2}$.²⁷ The decrease in amplitude is caused by the reduced ability of the surface electrons to screen the applied potential.

The function $\xi(q)$ which according to Eq. (31) characterizes the near-adiabatic surface excitations, is shown in Fig. 5 for several bulk densities. These results are obtained from the slopes of $\text{Im}g(q, \omega)$ calculated within the TDLDA for $\omega \sim 0.1 \text{ eV}$. Quasistatic evaluations of $\xi(q)$ based on Eq. (32) using $\phi_{\text{scf}}(z, q, 0)$ are in excellent agreement with these results. At small q , the functions $\xi(q)$ extrapolate very well to the coefficients ξ_s (34) derived in the long-wavelength limit.²⁸ This region will be discussed in Sec. IV D.

At large q , the surface response is seen to become very small when $q \approx 1.5k_F$. Such a cutoff is to be expected since the metal electrons are no longer able to screen the rapidly varying external potential $\sim e^{qz}$. Moreover, q should not exceed the decay constant of the electronic states and Green's functions in the vacuum. In any case, large q vectors are not important except at very short particle-surface distances. The assumption of negligible overlap with the metal states then ceases to be valid.

The maximum of $\xi(q)$ at intermediate values of q is a consequence of the increasing amplitude of ϕ_{ext} near the centroid of the induced charge density. If this effect is approximately accounted for by multiplying $\xi(q)$ by e^{-2qz_1} ,

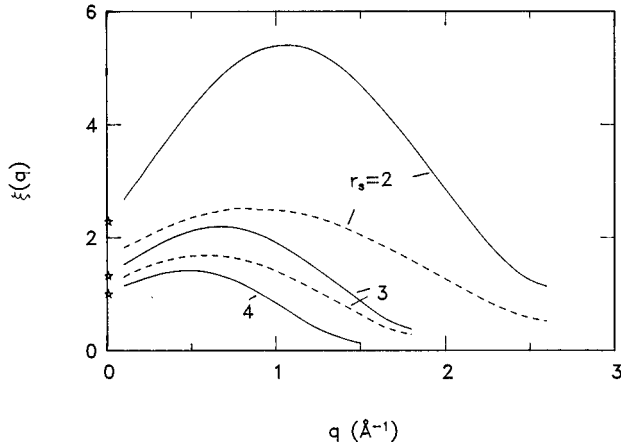


FIG. 5. Variation of $\xi(q)$ with parallel momentum for several bulk densities. Solid curves, standard jellium model; dashed curves, stabilized jellium model. The symbols at $q=0$ denote the standard jellium values of ξ , defined in Eq. (34). The Fermi wave vectors are $k_F=1.8, 1.2,$ and 0.9 \AA^{-1} for $r_s=2, 3,$ and 4 , respectively.

the product $\bar{\xi}(q)$ is indeed a monotonically decreasing function of q , just as one would expect on physical grounds.

It is well known that, because of the neglect of the lattice potential, the jellium model has certain shortcomings that affect the shape of the surface density profiles. In particular, for $r_s < 4$, the work functions are too small. Accordingly, the density profiles are too diffuse and too polarizable. The so-called stabilized jellium model²⁹ includes the pseudopotential of the metal ions in an average manner and leads to significantly improved work functions.

In Fig. 6 the equilibrium densities of the standard jellium model are compared with those of the stabilized jellium model. Although the differences might appear small, they nevertheless have a considerable influence on the electronic surface excitation spectra. This is illustrated in Fig. 5, which also shows the coefficient $\xi(q)$ for the stabilized jellium model for $r_s=2$ and $r_s=3$ (the results for $r_s=4$ are nearly unchanged). (See also Table I.) Since the equilibrium density of these surfaces is less diffuse than for standard jellium, the probability of exciting electron-hole pairs is reduced. For $r_s=2$, the maximum of $\xi(q)$ is about a factor of 2 smaller, while for $r_s=3$, the reduction is about 25%. These results demonstrate the remarkable sensitivity of the surface loss function to the electronic surface properties. Finite or infinite potential barrier models tend to have far too stiff density profiles and grossly underestimate the probability for electron-hole pair creation.

D. Long-wavelength limit

At finite frequency, the surface response function $g(q, \omega)$ has the long-wavelength expansion^{20,21}

$$g(q, \omega) = \frac{\epsilon - 1}{\epsilon + 1} \left(1 + \frac{2\epsilon}{\epsilon + 1} qd(\omega) + \dots \right). \quad (40)$$

Here $\epsilon(\omega)$ is the Drude dielectric function of the bulk metal and $d(\omega)$ the centroid of the screening charge induced by a

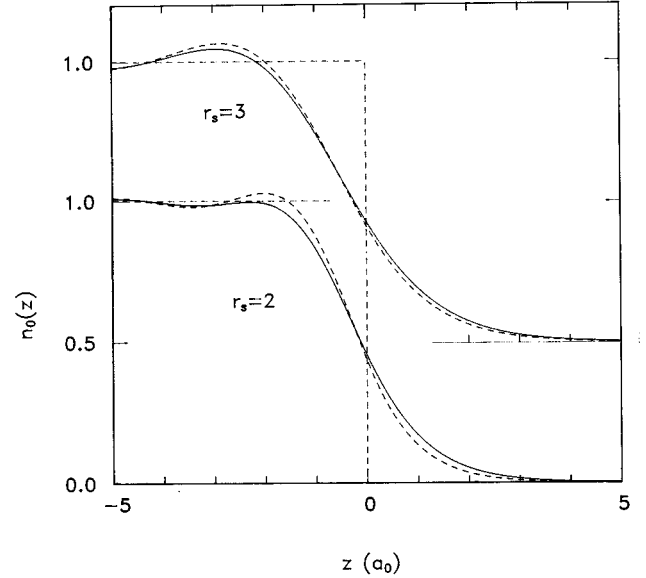


FIG. 6. Ground state density profiles for semi-infinite jellium surfaces. Solid curves, standard jellium; dashed curve, stabilized jellium.

uniform electric field oriented normal to the surface. At low frequencies (as long as $q \ll \omega/v_F$, i.e., $\eta \gg 1$), the above expansion simplifies to

$$g(q, \omega) = 1 + 2qd(\omega) + \dots, \quad (41)$$

and the imaginary part of $d(\omega)$ may be parametrized as

$$\text{Im}d(\omega) = \frac{\omega}{k_F \omega_p} \xi. \quad (42)$$

TABLE I. $\xi(q)$ for stabilized jellium surfaces as calculated within the TDLDA.

$q \text{ (\AA}^{-1}\text{)}$	$r_s=2$	$r_s=2.67$	$r_s=3$	$r_s=4$
0.0	1.70	1.35	1.19	1.02
0.1	1.82	1.45	1.30	1.14
0.2	1.97	1.55	1.44	1.25
0.3	2.11	1.65	1.54	1.34
0.4	2.24	1.74	1.62	1.40
0.5	2.35	1.81	1.68	1.42
0.6	2.42	1.85	1.69	1.38
0.7	2.48	1.84	1.67	1.30
0.8	2.52	1.81	1.61	1.18
0.9	2.51	1.75	1.53	1.02
1.0	2.48	1.66	1.41	0.84
1.2	2.38	1.42	1.12	0.47
1.4	2.17	1.12	0.81	0.21
1.6	1.90	0.80	0.47	
1.8	1.60	0.50	0.28	
2.0	1.26	0.30		
2.2	0.94			
2.4	0.67			
2.6	0.50			

The coefficient ξ is given by the golden rule expression

$$\xi = \frac{k_F \omega_p}{\pi^3} \lim_{\omega \rightarrow 0} \int_0^{k_F} dk_z \frac{1}{k_z'} |k_z' \phi_{\text{scf}}(k_z)|^2, \quad (43)$$

with $k_z' = (k_z^2 + 2\omega)^{1/2}$.

As shown by Persson and Zaremba,²¹ at low frequencies, the local potential may be separated as $\phi_{\text{scf}} = \phi_s + \phi_b$, where the short-range surface potential can be taken in the static limit, i.e., $\phi_s(z, q=0, \omega=0)$, and the long-range bulk potential is given by $\phi_b(z, q=0, \omega) = -4\pi z / (\epsilon + 1)$. According to this decomposition, the coefficient ξ may be split into surface, bulk, and interference terms as

$$\xi = \xi_s + \xi_b + \xi_i. \quad (44)$$

Since ξ_s can be derived from Eq. (43) by setting $k_z' = k_z$, this term coincides with the coefficient defined in Eq. (34). Thus, as pointed out above, the functions $\xi(q)$ plotted in Fig. 5 extrapolate at small q to the values ξ_s . The reason is that $\xi(q)$ is evaluated at sufficiently small ω that $\eta \ll 1$. On the other hand, the total ξ corresponds to first taking the small- q limit and subsequently letting ω become small, such that $\eta \gg 1$. Because of the discontinuity of the bulklike excitations at $\eta = 1$, these two limiting processes differ. At the frequency at which the results shown in Fig. 5 are evaluated (0.1 eV), this discontinuity occurs at $q = 0.01 \text{ \AA}^{-1}$, i.e., in a range that is irrelevant for the friction phenomena considered in this paper.

E. Approximate response treatments

In a previous paper,¹⁵ the low-frequency electronic excitations of jellium surfaces had been investigated following a different procedure: In the first step, rather than using a response formulation, the static induced density $n_1(\vec{r})$ was calculated by including the periodic potential $\phi_{\text{ext}}(\vec{r}) = -(2\pi/q)e^{iq_{\parallel} \cdot \vec{r}_{\parallel} + qz}$ in the LDA ground-state Hamiltonian. As mentioned above, this procedure gives densities in excellent agreement with the real part of those obtained at low ω by solving the response equation (19). In the second step, the coefficient $\xi(q)$ of the transition rate was evaluated from Eq. (32), with ϕ_{scf} constructed from n_1 and approximating $\phi_{\text{scf}} \approx \phi_{\text{ext}} + \phi_{\text{est}}$.

In order to illustrate the importance of the omitted exchange-correlation potential ϕ_{xc} for the surface excitations, we compare in Fig. 7 the new consistent results for $\xi(q)$ with the previous approximate ones. [Note that in Ref. 15 $\xi(q)$ is normalized in such a manner that the origin of the z coordinate is placed at the position z_1 of the static image plane, i.e., the functions $\bar{\xi}(q) = \xi(q)e^{-2qz_1}$ are plotted. We do not use this normalization here.] The neglect of ϕ_{xc} is seen to cause a significant underestimate of the surface loss function. As illustrated in Fig. 8, in the surface region $z = -1, \dots, 4a_0$, where the electronic transition occurs, ϕ_{xc} is negative so that the full ϕ_{scf} is much larger than the Coulomb part of it. For $r_s = 2$ the consistent $\xi(q)$ near its maximum is about twice as large as the approximate function, while for $r_s = 3$ the new $\xi(q)$ is nearly four times larger. The differences become even larger for lower bulk densities.

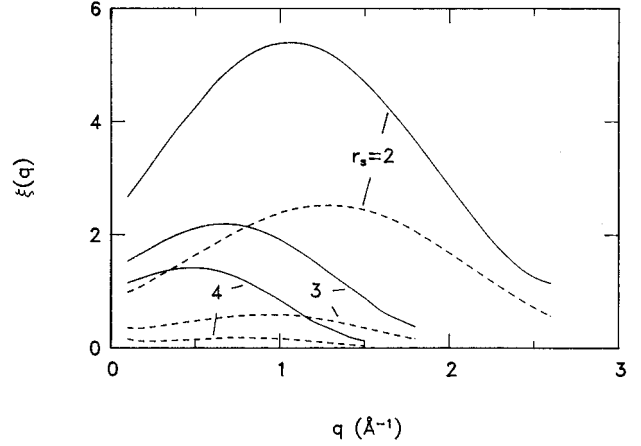


FIG. 7. Variation of $\xi(q)$ with parallel momentum for standard jellium surfaces (from top: $r_s = 2, 3, 4$). Solid curves, TDLDA; dashed curves, quasistatic results with ϕ_{scf} replaced by $\phi_{\text{ext}} + \phi_{\text{est}}$.

Another commonly made approximation uses the RPA, where the induced exchange-correlation potential is neglected also in the evaluation of the induced density. As shown in Fig. 9, this approximation leads to an appreciable underestimate of $\xi(q)$ since the effective interaction potential in the RPA is too strong. The surface density then appears much less polarizable than in the TDLDA, with accordingly smaller excitation probabilities. These discrepancies underline again the importance of employing a consistent response description.

V. SLIDING FRICTION OF IONS: K ON Cu

At large ion-surface separations, the electronic friction is dominated by bulk processes. The surface response function can then be expressed in terms of the bulk dielectric function. In the case of a Drude metal one has for $\omega \ll \omega_p$

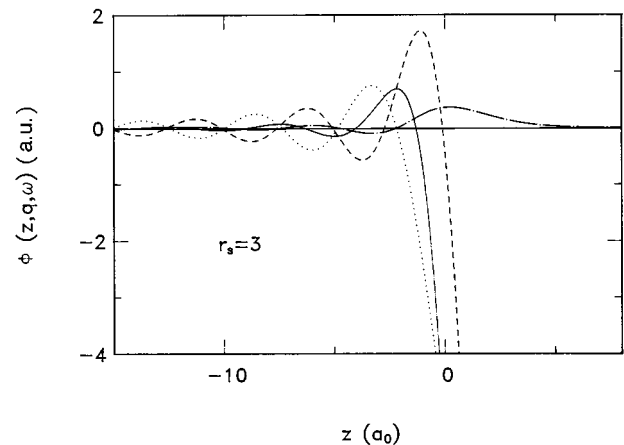


FIG. 8. Solid curve, real part of the self-consistent local potential $\phi_{\text{scf}}(z, q, \omega)$ at 0.1 eV and $q = 0.5 \text{ \AA}^{-1}$, as calculated within the TDLDA ($r_s = 3$); dashed curve, Coulomb potential $\phi_{\text{ext}} + \phi_{\text{est}}$; dotted curve, exchange-correlation potential ϕ_{xc} ; dot-dashed curve, induced density n_1 .

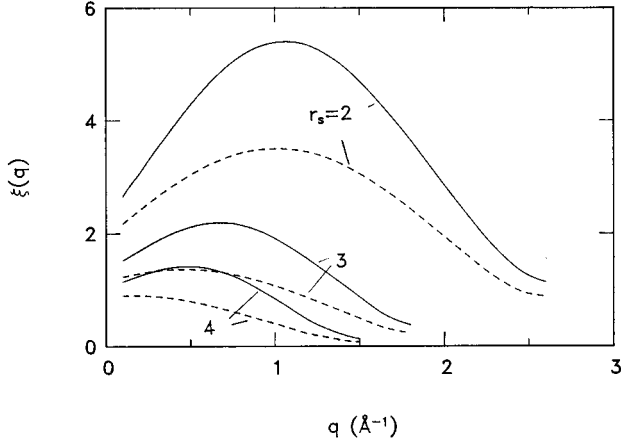


FIG. 9. Variation of $\xi(q)$ with parallel momentum for standard jellium surfaces (from top: $r_s=2,3,4$). Solid curves, TDLDA; dashed curves, RPA response treatment.

$$\text{Im}g(q, \omega) = \text{Im} \frac{\epsilon(\omega) - 1}{\epsilon(\omega) + 1} = \frac{4\omega\omega_F}{k_F l \omega_p^2}, \quad (45)$$

where l is the electronic mean free path. Thus

$$\eta_{\perp} = \frac{Q^2}{M} \frac{1}{4d^3} \frac{4\omega\omega_F}{k_F l \omega_p^2}. \quad (46)$$

This contribution to the damping rate accounts for bulk electron-hole pair creation due to impurities, phonons, and the lattice potential.

At short distances, surface contributions to η_{\perp} that arise from the nonlocal response of the metal become important. Using the low-frequency form of $g(q, \omega)$ given in Eq. (33), the friction coefficient can be expressed as

$$\eta_{\perp} = \frac{Q^2}{M} \frac{2}{k_F \omega_p} \frac{6}{(2d)^4} F(d), \quad (47)$$

where d is measured with respect to the jellium edge and the dimensionless ionic friction integral $F(d)$ is defined as

$$F(d) = \frac{(2d)^4}{6} \int_0^{\infty} dq q^3 e^{-2qd} \xi(q). \quad (48)$$

This expression indicates that, for a given d , the surface loss function is required at q values at least up to $1/d$. The function $F(d)$ is shown in Fig. 10 for various bulk densities. At large ion-surface distances, $F(d)$ approaches ξ_s defined in Eq. (34).

As an application we consider the damping of the parallel frustrated translation of a charged alkali atom adsorbed on a metal surface.³⁰ The adatom is treated as a point charge of magnitude Q that oscillates parallel to the surface with a frequency ω . In the case of a low coverage of potassium atoms on Cu(100), the distance of the K nucleus from the effective jellium edge (half a lattice constant above the first plane of nuclei) is about $d=2.65$ Å. From the measured work function change at low coverage one can determine the effective charge as $Q \approx 0.88|e|$. With these parameters we find for stabilized jellium [$r_s=2.67$, $F(d)=1.65$]

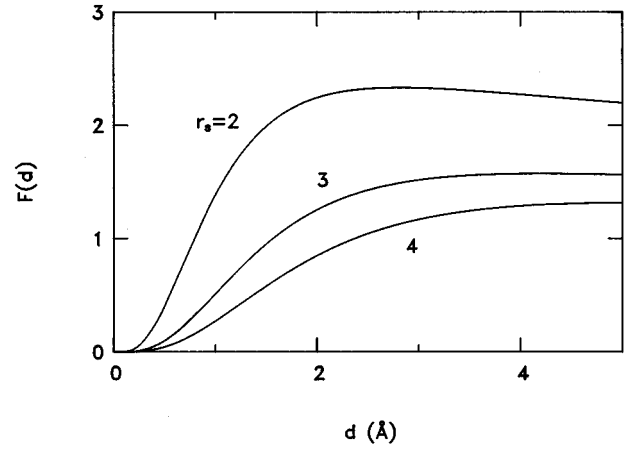


FIG. 10. Ionic friction integral $F(d)$ (48) as a function of ion-surface separation for several bulk densities. The metal is described using the stabilized jellium model and the dynamical response is treated within the TDLDA.

$$\eta_{\parallel} = 0.5\eta_{\perp} \approx 1.6 \times 10^9 \text{ s}^{-1}, \quad (49)$$

so that $\tau = 1/\eta_{\parallel} \approx 0.6 \times 10^{-9}$ s. This lifetime is about four times shorter than the value derived by Persson,³⁰ $\tau = 2.7 \times 10^{-9}$ s. About half of this difference is caused by the neglect of the exchange-correlation potential in the golden rule formula. The remaining factor of 2 originates in the incorrect reading of the function $\xi_s C(d-z_1)/(d-z_1)^4 \equiv F(d)/d^4$ from Fig. 3 of Ref. 15. [At $d=5 a_0=2.65$ Å, $C(d-z_1) \approx 0.5$ rather than 0.23 as quoted in Ref. 30.]

The new value of τ is of a similar size as the lifetime estimated by Persson for a ‘‘covalent’’ bond model ($\tau \approx 0.7 \times 10^{-9}$ s).³⁰ In the latter case, the K 4s level is broadened into a resonance due to the hybridization with the electronic states of the Cu substrate. This interaction leads to a damping since the partial filling of the resonance changes during the oscillatory motion of the ion.

We note here that there is an interesting relationship between the parallel friction coefficient and the surface resistivity associated with the adsorption of atoms on metal surfaces. As shown by Persson,³⁰

$$\eta_{\parallel} = \frac{e^2}{M} \frac{n^2}{n_a} l_f \rho_a, \quad (50)$$

where M is the mass of the adsorbed atoms, n the electronic density of the substrate, n_a the number of adatoms per unit area, and l_f the thickness of the metal film. The overlayer induced resistivity ρ_a can be expressed in terms of the d parameter for tangential surface currents via

$$\rho_a = \frac{\omega}{l_f n} \text{Im} d_{\parallel}(\omega), \quad (51)$$

so that

$$\eta_{\parallel} = \frac{e^2}{M} \frac{n}{n_a} \omega \text{Im} d_{\parallel}(\omega). \quad (52)$$

For realistic Na layers adsorbed on jellium with $r_s=2$ (corresponding to an Al substrate) Ishida and Liebsch³¹

evaluated the frequency dependence of $d_{\parallel}(\omega)$ and obtained at low ω $\text{Im } d_{\parallel}(\omega) = \zeta \omega_p / \omega$, with $10^3 \zeta = 6.2a_0$ at a coverage $c = 1/4$. The lattice constant of the overlayer square lattice at $c = 1$ is $a_{\parallel} = 6.684a_0$ and the distance of the Na nuclei from the substrate jellium edge $d = 3a_0 = 1.59 \text{ \AA}$. With these parameters, the lateral friction coefficient is

$$\eta_{\parallel} = \frac{m}{M} \frac{\omega_p^3}{4\pi n_a} \zeta = 2 \times 10^{10} \text{ s}^{-1}, \quad (53)$$

i.e., $\tau = 1/\eta_{\parallel} \approx 0.5 \times 10^{-10} \text{ s}$. This lifetime is about one order of magnitude smaller than the one derived above for K ions on Cu. In part, this reduction is caused by the shorter adsorbate-metal distance which according to Eq. (47) decreases τ like d^4 . Thus, $(d_{\text{Na}}/d_{\text{K}})^4 = (3/5)^4 \approx 0.13$. Other contributions should arise from the stronger broadening of the Na $4s$ resonance due to the hybridization with the metal states.

More recently, Ishida³² has calculated the surface resistivity ρ_a for a variety of chemisorbed overlayers and adsorbed atoms. Since these calculations include the covalent nature of the bond, it would be interesting to compare them with the present approach appropriate for ions outside the equilibrium density of the metal. In this manner one could separate the contributions to the friction coefficient due to bond formation and due to external charges.

For completeness we mention here that the lifetime of the CO stretch vibration on Cu evaluated in Ref. 15 should be decreased by about a factor of 1.6 as a result of the consistent response description. The new value for stabilized jellium ($r_s = 2.67$) is $\tau \approx 3.2 \times 10^{-12} \text{ s}$, if the dipole is assumed not to overlap with the surface electron density, and $\tau \approx 6.0 \times 10^{-12} \text{ s}$, if the dipole is located slightly within the density region. This latter lifetime agrees well with the TDLDA results by Eguluz.³³ The shorter measured value $\tau \approx 1.3 \times 10^{-12} \text{ s}$ (Ref. 34) is presumably caused by the additional damping due to the partial filling of the CO $2\pi^*$ level.³⁵

VI. SLIDING FRICTION OF PHYSORBED ATOMS: Xe ON Ag

Inserting the low-frequency behavior of $\text{Im}g(q, \omega)$ given in Eq. (33) into the friction coefficient (10) for physisorbed atoms, we find that η_i can be written in the form⁹ ($i = \parallel, \perp$)

$$\begin{aligned} \eta_i &= \frac{e^2}{M} \frac{2}{2\pi k_F \omega_p} \sum_{\vec{q}_{\parallel}} |V_i(\vec{q}_{\parallel})|^2 q^2 \xi(q) \\ &= \frac{e^2}{a_0} \frac{[k_F^3 \alpha(0)]^2}{(k_F d)^{10}} \frac{m}{M} \frac{\omega_F}{\omega_p} k_F a_0 I_i(d), \end{aligned} \quad (54)$$

where d is the distance of the atom from the jellium edge. The proportionality $\eta_i \sim 1/d^{10}$ agrees with the one found by Schaich and Harris.¹² The dimensionless atomic friction integrals $I_i(d)$ are defined as

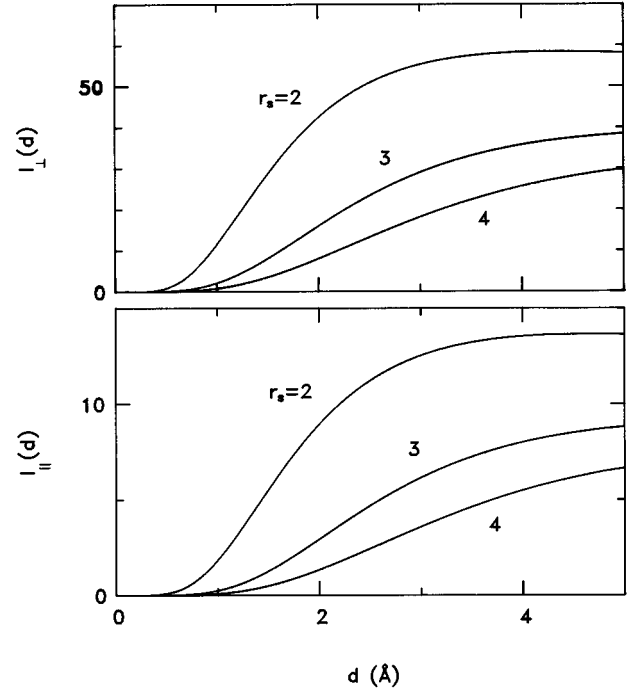


FIG. 11. Atomic friction integrals $I_{\perp}(d)$ and $I_{\parallel}(d)$ (55) as a function of atom-surface separation for several bulk densities. The metal is described using the stabilized jellium model and the dynamical response is treated within the TDLDA.

$$\begin{aligned} I_i(d) &= \frac{4d^{10}}{\pi^2} \int d^2q q^4 \xi(q) \\ &\times \left| \int d^2q' \frac{\vec{q}' \cdot \vec{q}'' - q' q''}{q' q'' (q + q' + q'')} Q_i'' e^{-(q' + q'')d} \right|^2. \end{aligned} \quad (55)$$

These functions are shown in Fig. 11 for various bulk densities. At large atom-surface distances, the $I_i(d)$ scale like the coefficients ξ_s defined in Eq. (34). Note that these functions are very much larger than the ones given in Ref. 9. The increase is partly caused by the inclusion of the exchange-correlation potential in the golden rule formula and, even more importantly, by the fact that in Ref. 9 the normalized coefficient $\bar{\xi}(q) \equiv e^{-2qz_1} \xi(q)$ instead of the full $\xi(q)$ was used in the evaluation of Eq. (55).

In the case of Xe atoms physisorbed on Ag(111) one has $d = 2.4 \text{ \AA}$. The static polarizability of Xe is $\alpha(0) = 4.0 \text{ \AA}^3$. Using the TDLDA results for $\xi(q)$ shown in Fig. 5, we find for stabilized jellium ($r_s = 3$) the parallel friction coefficient $\eta_{\parallel} \sim 3.4 \times 10^8 \text{ s}^{-1}$ in contrast to $\eta_{\parallel} \sim 0.4 \times 10^8 \text{ s}^{-1}$ in Ref. 9. The friction coefficient for the perpendicular motion is $\eta_{\perp} \sim 17.4 \times 10^8 \text{ s}^{-1}$ instead of $\eta_{\perp} \sim 2.5 \times 10^8 \text{ s}^{-1}$ using the approximate $\xi(q)$.

The calculated parallel friction coefficient η_{\parallel} is in approximate agreement with the values obtained from experiments for Xe on Ag: surface resistivity data yield $\eta_{\parallel} \sim 3 \times 10^8 \text{ s}^{-1}$,^{4,8} while recent quartz-crystal microbalance measurements give $\eta_{\parallel} \sim 8 \times 10^8 \text{ s}^{-1}$.¹⁷ For phonon-related friction, on the other hand, Persson and Nitzan¹⁰ estimated

$\eta_{\parallel} \sim 0.6 \times 10^8 \text{ s}^{-1}$ for isolated Xe atoms on Ag. This value should also be a reasonable approximation for fluid adsorbate layers. For incommensurate solid adsorbate layers, on the other hand, the phonon contribution to the friction is expected to vanish.³⁶ The friction coefficient arising from the van der Waals attraction is also significantly larger than the contribution due to the Pauli repulsion. The latter has been estimated by Persson at about $\eta_{\parallel} \sim 0.6 \times 10^8 \text{ s}^{-1}$.³⁰

The theoretical value of η_{\parallel} given above presumably represents a slight overestimate since the Xe atom is not completely outside the range of the electronic density profile. Moreover, the derivation of expression (6) implies some uncertainty. Also, as a result of the *s-d* hybridization, the surface polarizability of real Ag might be slightly smaller than that of the corresponding jellium model. We note, in addition, that for Xe there might exist some friction due to ‘chemical’ effects which result from the broadening of the Xe 6*s* level. Estimates of this mechanism yield $\eta_{\parallel} \sim 1.5 \times 10^8 \text{ s}^{-1}$.³⁰ For the lighter rare gas atoms, this effect should be negligible since the lowest unoccupied *s* level does not extend down to the Fermi energy.

VII. SUMMARY

The low-frequency electronic excitations at jellium surfaces were evaluated within the time-dependent density-functional approach. The consistent description of electron-electron interactions in the presence and absence of the external perturbation yields much larger excitation probabilities than approximate (and inconsistent) interaction treatments. For Xe sliding above a Ag surface, the friction coefficient associated with the van der Waals attraction is found to be in good agreement with recent experimental results obtained from surface resistivity and quartz-crystal microbalance measurements. The friction of alkali atoms on metal surfaces is also much larger than in previous approximate

treatments. These results demonstrate the importance of the electronic friction mechanism for atoms adsorbed on metal surfaces.

The dynamical response calculations discussed in the present work are carried out within the jellium model. We have found that, to excellent numerical accuracy, the TDLDA excitation spectra at small ω and finite q can be derived either from the golden rule expression (32) involving the local potential $\phi_{\text{scf}}(z, q, \omega)$, or from the surface loss function $\text{Im}g(q, \omega)$ which involves the induced density $n_1(z, q, \omega)$. This equivalence is of considerable practical importance for future evaluations of $\xi(\vec{q}_{\parallel})$ for realistic metals. Since the self-consistent potential ϕ_{scf} in the golden rule expression can be taken in the static limit, it can be derived from an extension of existing ground state electronic structure codes by applying a weak static potential of the form $\sim e^{i\vec{q}_{\parallel} \cdot \vec{r}_{\parallel} + qz}$.

Such external potentials represent a periodic perturbation in the surface region. If \vec{q}_{\parallel} is chosen as a simple fraction of the surface reciprocal lattice vectors, it should be relatively straightforward to find the static induced density $n_1(\vec{r})$ and the corresponding local potential $\phi_{\text{scf}}(\vec{r}, \omega=0)$. In view of the computational difficulties of evaluating the dynamical response of realistic metals, static response calculations at finite \vec{q}_{\parallel} should therefore be highly valuable for the analysis of phenomena involving low-frequency electronic excitations at metal surfaces. Such calculations might well become the next generation of surface response work. They would significantly complement the dynamical response of simple metal surfaces that has been of primary interest in the past.

ACKNOWLEDGMENT

It is a pleasure to acknowledge useful discussions with Bo Persson.

-
- ¹F.P. Bowden and D. Tabor, *Friction and Lubrication* (Methuen, London, 1967).
- ²*Physics of Sliding Friction*, edited by B.N.J. Persson and E. Tosatti (Kluwer, Dordrecht, 1996); *Fundamentals of Friction: Macroscopic and Microscopic Processes*, edited by I.L. Singer and H.M. Pollock (Kluwer, Dordrecht, 1992).
- ³J. Krim, D.H. Solina, and R. Chiarello, *Phys. Rev. Lett.* **66**, 181 (1991); J. Krim and A. Widom, *Phys. Rev. B* **38**, 12 184 (1988).
- ⁴C. Holzapfel, W. Akemann, and D. Schumacher, *Surf. Sci.* **227**, 123 (1990); D. Schumacher, *Surface Scattering Experiments with Conduction Electrons*, Springer Tracts in Modern Physics Vol. 128 (Springer-Verlag, Berlin, 1992).
- ⁵M. Cieplak, E.D. Smith, and M.O. Robbins, *Science* **265**, 1209 (1994); M.O. Robbins, in *Physics of Sliding Friction* (Ref. 2).
- ⁶B.N.J. Persson, *Comments Condens. Matter Phys.* **17**, 281 (1995).
- ⁷C. Daly and J. Krim, *Phys. Rev. Lett.* **76**, 803 (1996); J. Krim and C. Daly, in *Physics of Sliding Friction* (Ref. 2).
- ⁸D. Schumacher, in *Physics of Sliding Friction* (Ref. 2).
- ⁹B.N.J. Persson and A.I. Volokitin, *J. Chem. Phys.* **103**, 8679 (1995).
- ¹⁰B.N.J. Persson and A. Nitzan, *Surf. Sci.* **367**, 261 (1996).
- ¹¹A. Liebsch, *Electronic Excitations at Metal Surfaces* (Plenum, New York, 1997).
- ¹²W.L. Schaich and J. Harris, *J. Phys. C* **11**, 65 (1981).
- ¹³L.S. Levitov, *Europhys. Lett.* **8**, 499 (1989).
- ¹⁴J.B. Sokoloff, *Phys. Rev. B* **52**, 5318 (1995).
- ¹⁵A. Liebsch, *Phys. Rev. Lett.* **54**, 67 (1985).
- ¹⁶A. Zangwill and P. Soven, *Phys. Rev. A* **21**, 1561 (1980); M.J. Stott and E. Zaremba, *ibid.* **21**, 12 (1980); G. Mahan, *ibid.* **22**, 1780 (1980).
- ¹⁷J. Krim (unpublished).
- ¹⁸W.L. Schaich, *Solid State Commun.* **15**, 357 (1974); E.G. D’Agliano, O. Kumar, W.L. Schaich, and H. Suhl, *Phys. Rev. B* **11**, 2122 (1975); B.N.J. Persson, *J. Phys. C* **11**, 4251 (1978).
- ¹⁹J. Harris and R.O. Jones, *J. Phys. C* **6**, 3585 (1973); **7**, 3751 (1974).
- ²⁰P.J. Feibelman, *Prog. Surf. Sci.* **12**, 287 (1982).
- ²¹B.N.J. Persson and E. Zaremba, *Phys. Rev. B* **31**, 1863 (1985).
- ²²R.R. Chance, A. Prock, and R. Silbey, *Adv. Chem. Phys.* **37**, 1 (1978); B.N.J. Persson and W.L. Schaich, *J. Phys. C* **14**, 5583 (1981).
- ²³E.K.U. Gross and W. Kohn, *Phys. Rev. Lett.* **55**, 2850 (1985); **57**,

- 923(E) (1986); N. Iwamoto and E.K.U. Gross, Phys. Rev. B **35**, 3003 (1987).
- ²⁴A. Liebsch, Phys. Rev. B **32**, 6255 (1985).
- ²⁵A. Liebsch, J. Phys. C **19**, 5025 (1986).
- ²⁶N.D. Lang and W. Kohn, Phys. Rev. B **7**, 3541 (1973).
- ²⁷J.F. Dobson and G.H. Harris, Phys. Rev. B **27**, 6542 (1983).
- ²⁸A. Liebsch, Phys. Rev. B **36**, 7378 (1987).
- ²⁹J.P. Perdew, H.Q. Tran, and E.D. Smith, Phys. Rev. B **42**, 11 627 (1990); H.B. Shore and J.H. Rose, Phys. Rev. Lett. **66**, 2519 (1991).
- ³⁰B.N.J. Persson, Phys. Rev. B **44**, 3277 (1991).
- ³¹H. Ishida and A. Liebsch, Phys. Rev. B **45**, 6171 (1992).
- ³²H. Ishida, Phys. Rev. B **49**, 14 610 (1994); **52**, 10 819 (1995); Surf. Sci. **363**, 354 (1996).
- ³³A.G. Eguiluz, Phys. Scr. **36**, 651 (1987).
- ³⁴R. Ryberg, Surf. Sci. **114**, 627 (1982).
- ³⁵B.N.J. Persson and M. Persson, Solid State Commun. **36**, 175 (1980).
- ³⁶J.B. Sokoloff, Phys. Rev. B **42**, 760 (1990).